IAHR
24th Symposium on Hydraulic Machinery and Systems
OCTOBER 27-31, FOZ DO IGUASSU


# A CFD STUDY OF A FINITE TEXTURED JOURNAL BEARING

Samuel Cupillard[1*], Michel J. Cervantes[2] and Sergei Glavatskih[1]

[1] Division of Machine Elements, Luleå University of Technology, SE-97187 Luleå, Sweden
[2] Division of Fluid Mechanics, Luleå University of Technology, SE-971 87 Luleå, Sweden
[*] e-mail: samcup@ltu.se, tel.: +46-920-491734

## ABSTRACT
An analysis of a lubricated journal bearing is performed with special attention to the influence of textured surfaces which may improve hydrodynamic performance. The bearing is subjected to an external applied load and the force balance is fulfilled with the force of the flow acting on the bearing. The position of the shaft is fixed whereas the bearing, centred at the starting time, moves under the forces until equilibrium is reached. A mesh deformation technique is used with CFD (Computational Fluid Dynamics) in order to perform the simulations. The flow is laminar, isothermal, three-dimensional (3D) and unsteady. Cavitation is taken into account. Results are analysed with smooth and textured surfaces on the bearing. Friction force and eccentricity ratio are compared for different configurations.

It is found that shallow grooves under light loading ($\varepsilon < 0.15$) enhance the minimum film thickness while reducing the friction force. Under high loading ($\varepsilon > 0.5$), deep grooves are able to reduce the friction force despite a reduced minimum film thickness. For the second case, the predicted performance is superior to those of a smooth journal bearing with thinner lubricant.

**KEY WORDS**: Texturing, journal bearing, mesh deformation, friction

## INTRODUCTION
Journal bearings with modified surface shape have attracted considerable interest as it is a promising way to enhance their hydrodynamic performance. A different bearing shape leads to a different flow pattern in the lubricant film and new characteristics must be considered. Optimisation of these surface shapes is a rather long process compared with the short-term studies which, in fact, already showed improved performance in some cases [1–9]. A trend on where and how implanting such texture has started to emerge since modification of the bearing shape has already been investigated both numerically and experimentally.

Etsion [1] showed the potential of surface texturing in different applications such as seals, pistons rings and thrust bearings. Journal bearings can also be textured in the same way, therefore references below are devoted to them. The bearing surface can be textured in two different ways: full texturing where a regular shape is reproduced all over the bearing surface or partial texturing which is realised only on a part of the bearing surface. Lin [2] studied a fully textured finite journal bearing with three-dimensional irregularities. One of his findings was that with increased asperity height the load capacity of the bearing increases and the friction coefficient decreases. In his case, the fluid film is actually reduced when the asperities are introduced. Li and Braun [3] investigated the modeling of the flow in a journal bearing with diamond-knurled stator surface. They found that the load carrying capacity of the knurled bearing is smaller than the one of the smooth bearing at high eccentricities whereas about the same for eccentricity ratios lower than 0.5. Kato and Obara [4] numerically

analysed an isothermal microgrooved bearing under the whole range of eccentricity ratios and claimed that the dynamic characteristics of the journal bearing were improved whereas the static characteristics (load carrying capacity and friction coefficient) were not changed by the microgrooving. The microgrooves were placed along the circumferential direction over the entire bearing surface. The same microgrooved bearing was tested experimentally by Kumada et al [5] who showed some advantages even though a slightly higher friction coefficient was observed. The microgrooving was able to increase the cooling effect of the oil flow. The oil-retaining property of the microgrooved bearing was suggested to be superior. In the study of Ausas et al [6], a fully textured bearing with an array of 50×5 squared textures slightly increases the eccentricity ratio and the friction torque compared with a smooth bearing under the same load. Tala-Ighil et al [7] analysed a journal bearing textured with spherical dimples at an eccentricity ratio of about 0.6 and concluded that the presence of texture on the whole bearing surface has a negative influence on the performance whereas a partially textured bearing can have positive effects on the bearing characteristics. A texture localized in the diverging part of the bearing (from minimum to maximum film) enables higher fluid film and lower friction torque. In a previous study of Cupillard et al [8], positive effects of a partially textured journal bearing were shown. Effects of dimple dimensions were analysed and improvement of the hydrodynamic performance was realized due to the texture. Implanting a texture either in the maximum pressure or in the maximum film zone was able to reduce the friction coefficient or improve the load carrying capacity respectively. This 2D study was confirmed by the same trend for a 3D case although a lower gain in performance was observed. Partial texturing of such bearings seems to be promising. Nevertheless, more understanding is needed for texture configurations where improvement can be achieved.

Two solutions have been proposed for improving the performance of a journal bearing [8]. The first one is to introduce dimples or grooves such as to decrease the losses locally in order to build up extra pressure and then increase the load carrying capacity. The second one consists of introducing a texture of larger depth in order to reduce the friction more than the load carrying capacity, the friction coefficient may then been reduced. These two alternatives have been investigated for a 2D journal bearing (or infinite bearing) and only verified for a 3D static case [8]. In reality the load is applied and the shaft is moving until a final equilibrium is reached when the forces balance themselves.

The goal of this paper is to test these two texture configurations where an initially centred shaft is subjected to a load. The final steady state position is then analysed. This study is performed with CFD for a laminar, unsteady, 3D and isothermal flow. A mesh deformation technique is used to recalculate the lubricant film thickness at each time step. The focus of the work is to determine the effect of surface texture on hydrodynamic lubrication in terms of the minimum film thickness and the friction force. Two groove configurations corresponding to two different loadings of the shaft are investigated.

## NUMERICAL MODEL

### Geometries used and boundary conditions

Two geometries are considered: a smooth and a textured one. The smooth geometry is considered with both the shaft and the bearing smooth. The textured geometry is considered with a smooth shaft and a textured bearing. The dimensions of the smooth geometry and the lubricant properties are identical to that in the experimental work of Jakobsson and Floberg [10]. The flooded bearing has a length $L$ = 0.133 m, shaft radius $R_s$ = 0.05 m, radial clearance $c$ = 0.145 mm and shaft angular velocity $\omega$ = 48.1 rad/s. Above saturation pressure, the lubricant has a density of 840 kg/m$^3$ and a dynamic viscosity of 0.0127 Pa s. At the bearing and shaft surfaces, no-slip boundary conditions are assumed: the fluid moves with the same velocity as the surface considered. A symmetry condition is applied on the mid-plan of the

bearing in order to simulate only half of the domain. On the side of bearing, the pressure is set at the ambient value, i.e. the relative pressure is set to zero.

The surface texture adopted in this work is the same as in the previous work [8]: a series of ten grooves is created on the bearing surface along the axial direction from the mid-plan of the bearing. The cross section in the mid-plan of the bearing is represented in Figure 1. The distance between grooves does not exceed 10% of their width. The cross-section of the texture is chosen to be circular as this would be relatively easy to manufacture and quite convenient from a meshing point of view. A groove is characterized by its width ($w$), depth ($d$) and length ($l$). Two different groove depths are chosen, referring to deep and shallow grooves as in the reference [8]. For deep grooves, $d$ = 1.15 mm; for shallow grooves, $d$ = 45 μm. The groove length is varied for these 2 configurations and the ratio between groove and bearing length ($l/L$) is considered. Two different positions of the texture are also considered depending on the groove depth used. The shallow grooves operating for light loading are located at the maximum film. This configuration is supposed to give higher load carrying capacity [8, 9]. The grooves are centred around the $x$-axis at negative $y$-coordinates. The center of the first groove is positioned at θ = 68.4°. The deep grooves for high loadings are located in the maximum pressure zone which is load dependent. This is shown to lead to a lower coefficient of friction [8]. In our case, for a load of 1125 N, the center of the first groove is positioned at θ = 190°.

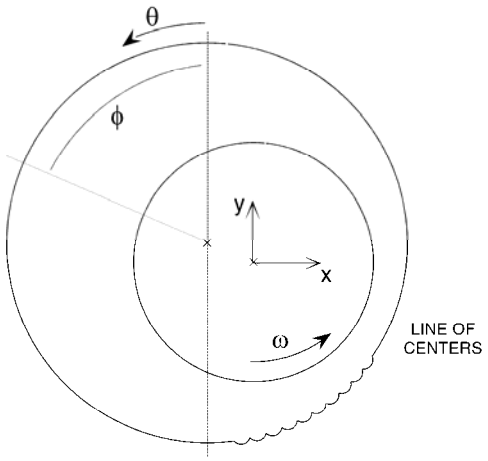


Figure 1: Cross section of the geometry in the mid plan, high loading configuration (the size of radial clearance is exaggerated)

**Equations**

The code used to model the problem is CFX 11.0. The Navier-Stokes equations, momentum equation (1) coupled with the continuity equation (2), are solved over the domain, using the finite volume method. The 3D flow is considered isothermal and laminar. Transient simulations are performed.

$$\frac{\partial(\rho u_i)}{\partial t} + \frac{\partial(\rho u_i u_j)}{\partial x_i} = -\frac{\partial P}{\partial x_i} + \frac{\partial}{\partial x_j}\left(\mu\left(\frac{\partial u_i}{\partial x_j} + \frac{\partial u_j}{\partial x_i}\right)\right) \quad (1)$$

$$\frac{\partial \rho}{\partial t} + \frac{\partial(\rho u_i)}{\partial x_i} = 0 \quad (2)$$

At low pressure values the lubricant enters in a regime of cavitation. The cavitation model used, allowing sub-ambient pressure, is based on a density-pressure relation on the same manner than in [11]. When the pressure drops under the cavitation pressure Pcav, the density decreases according to the following law:

$$\rho = \begin{cases} \rho_0 & if\ P > P_{cav} \\ \rho_0 \left[ 3\left(\frac{P}{P_{cav}}\right)^2 - 2\left(\frac{P}{P_{cav}}\right)^3 \right] & if\ P \le P_{cav} \end{cases} \quad (3)$$

Contrary to two phases flow cavitation models, this model does not predict an amount of vapor in the cavitation zone or a mixture air-lubricant but assumes a single phase with a varying density. This model has the advantage to be more stable and convergence is easier to get.

The bearing is subjected to the applied load and the resulting force of the fluid. The shaft is kept in a fixed position. From Newton's second law, an equation of movement is derived along x and y axis.

$$m_S \frac{d\vec{V}_S}{dt} = \vec{F} + \vec{F}_L \quad (4)$$

where $\vec{F} = (F_x, F_y)$ is the force of the flow acting on the bearing surface and $\vec{F}_L$ is the applied load along the y-direction.

After projection along the *x*- and *y*-axis and discretisation, the equations of movement become:

$$d_x(t) = \alpha\left( \Delta t^2 \frac{F_x(t-1)}{m_S} + \Delta t \cdot V_x(t-1) \right) + d_x(t-1) \quad (5)$$

$$d_y(t) = \alpha\left( \Delta t^2 \frac{F_y(t-1) + F_L(t-1)}{m_S} + \Delta t \cdot V_y(t-1) \right) + d_y(t-1) \quad (6)$$

where $d_x(t)$, $d_y(t)$ are the displacement components of the bearing at the time t; $V_x(t)$, $V_y(t)$ are the velocity components of the bearing at the time t and $\Delta t$ is the time step. $\alpha$ is a relaxation parameter which is introduce and taken to 0.1 in order to stabilize the numerical simulations.

These displacements are set at the bearing boundary. The nodes at the shaft boundary are stationary. With the displacement applied on the nodes of the bearing boundary, the motion of all remaining nodes of the domain is diffused and the spacing of the initial mesh is not changed much. The integral conservation of the equations must be modified as the control volumes deform in time. The transient term accounts for the rate of change of the deforming control volume. As an example, the integration of the continuity equation over a control volume becomes:

$$\frac{d}{dt}\int_{V(t)} \rho dV + \int_S \rho(u_i - w_i) dn_i = 0 \quad (7)$$

where $w_i$ is the velocity of the control volume boundary.

The principle is the same for the transient term of the momentum equation where the velocity of the control volume boundary is also taken into account.

**Solution procedure**

The meshing of the domain is performed in order to solve the momentum and continuity equations over each grid cell. The high resolution scheme in CFX 11.0 is used to discretise the advection term. This scheme gives second order accuracy gradient resolution while keeping solution variables physically bounded. It only reduces to a first order scheme close to discontinuities.

This space discretization induces an error into the numerical simulation. An estimation of this error is possible with a Richardson extrapolation. This method is used to investigate the value of the eccentricity ratio and the friction force for the smooth geometry with an applied load $W$ = 1125 N. As the real value of the eccentricity ratio and friction force are not known, this method is expected to give an approximation of the exact values and enables estimation of the grid error [12]. The values of the eccentricity ratio and friction force are plotted in Figure 2 for grids of 3 600, 28 800 and 230 400 elements with refinements close to the bearing, shaft and side surfaces. The value of the error for the finest grid is estimated to be around 5% for the eccentricity ratio and 1.8% for the friction. These errors are rather small and the results are considered to be reliable. This grid of 20×480×24 elements in (r,θ,z) directions respectively is used for the smooth case in the following work scope. The grids of the different textured cases are similar but refined slightly more in the groove zone.

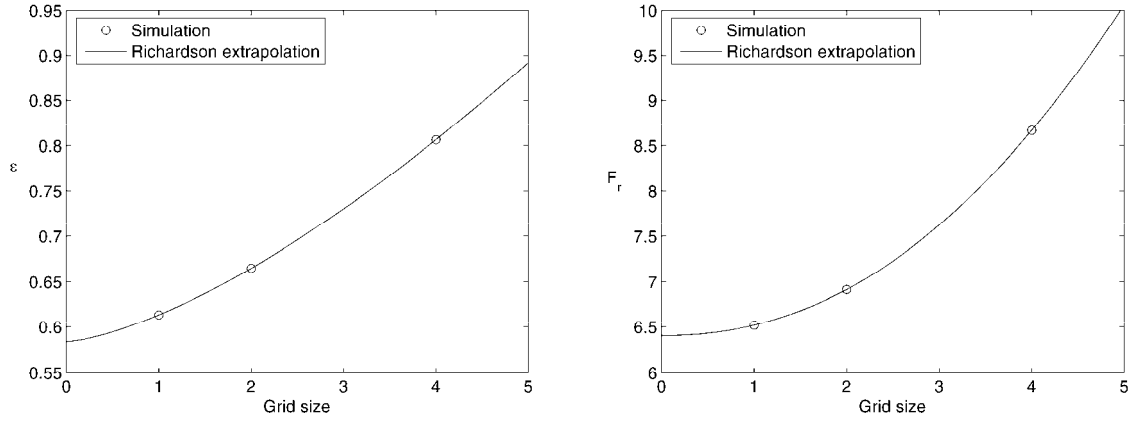


(a) Eccentricity ratio (b) Friction

Figure 2: Mesh dependency study

At t = 0 s, the bearing is centred and the eccentricity is zero. The load ($W$) is applied gradually in $t_W$ = 0.01 s (Eq. 8) so as to keep numerical stability.

$$F_L = \begin{cases} W\left[3\left(\frac{t}{t_W}\right)^2 - 2\left(\frac{t}{t_W}\right)^3\right] & if\ t \le t_W \\ W & if\ t > t_W \end{cases} \quad (8)$$

The bearing will theoretically be in movement until the forces balance themselves. After a sufficient amount of iteration, the position of the bearing stabilizes, the force of the flow converges to the opposite of the applied load and the velocity of the bearing becomes close enough to zero to consider that the steady state is reached. The time step (Δt) has to be small enough to obtain convergence of the transient run. For high loadings, Δt = 0.05 ms and the steady state is established at around t = 1 s for the smooth case. For light loadings, Δt = 0.2 ms and the steady state is established at around t = 0.2 s for the smooth case.

For light loading, cavitation is not expected since pressure does not reach the saturation pressure level. Therefore, the final position of the bearing is theoretically located on the x-axis

(horizontal axis). When cavitation does not occur, the system becomes less stable and much more time is required to reach the equilibrium state since the locus of the bearing converges at a very slow rate (the damping is quite weak). To simplify the numerical process, the degrees of freedom of the system are reduced to the displacement along the *x*-axis. The equation of movement is then:

$$d_x(t) = \alpha\left(\Delta t^2 \frac{-F_y(t-1) - F_L(t-1)}{m_S} + \Delta t \cdot V_x(t-1)\right) + d_x(t-1) \tag{9}$$

The simulation of the textured bearing is started from the final position of the smooth case so that steady state is reached within less time. For all the simulations the residuals of the momentum and mass conservation equations reach a level low enough, meaning that those equations are converged.

The results and comparison between smooth and textured cases can then be analysed in terms of eccentricity, minimum film thickness and friction force (10).

$$F_r = \frac{Torque}{R_S} \tag{10}$$

**Validation of the computational results**

The smooth model is validated with the experimental results of Jakobsson and Floberg [10]. The fluid saturation pressure used in the model is $P_{cav}$ = 30 kPa, which corresponds to a sub-ambient pressure. In the experiments, the bearing was loaded with a constant load of 2250 N. Half of the load is then applied to the half domain. The results can be seen in Figure 3. Pressure predicted by computational fluid dynamics (CFD) closely follows experimental points including the cavitation region. Very good agreement between CFD and experimental results is observed. The eccentricity ratio of 0.613 obtained in the numerical simulation matches well the experimental one which was around 0.61. This cavitation model is used in all the simulations when cavitation is expected.

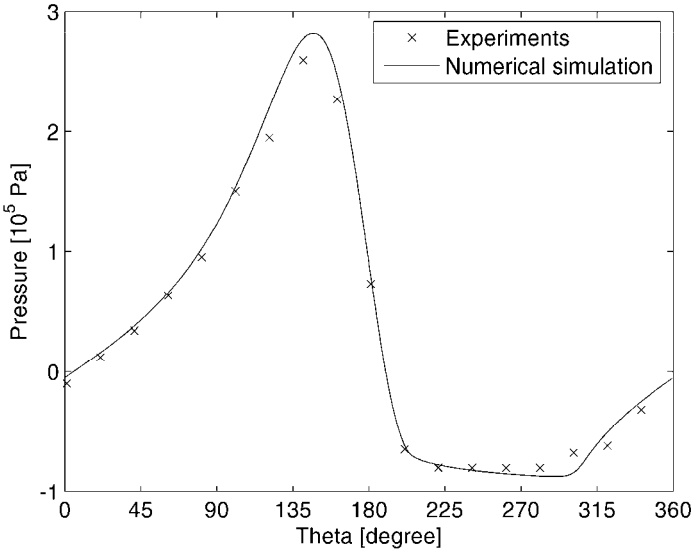


Figure 3: Experimental and numerical pressure profiles at z/l = 0.1 with the reference *z*-coordinate at the centre-line of the bearing

**RESULTS**

Two configurations were then tested: high loading conditions where $W$ = 1125 N and deep grooves ($d$ = 1.15 mm) are used in the region of maximum pressure and, light loading conditions where $W$ = 200 N and shallow grooves ($d$ = 45 μm) are implanted in the region of maximum film thickness.

**Light loading**

The bearing is loaded with 200 N and released from its initial position. The textured bearing is such that the groove lengths are $l/L$ = 0.5, 0.6, 0.7, 0.8, 0.9 and 1. The bearing has a unilateral displacement along the x-axis. The eccentricity ratio is plotted for different texture lengths as a function of time, see Figure 4.

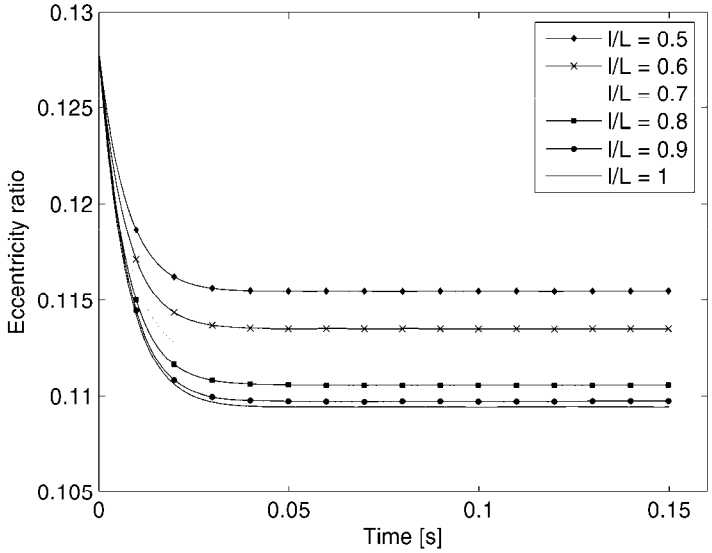


Figure 4: Eccentricity ratio as a function of time

Compared with the smooth bearing, the eccentricity reduces with the groove length. In other words, the grooves are able to increase the minimum film. This decrease in the eccentricity ratio together with a reduction in friction force can be seen in Figure 5.

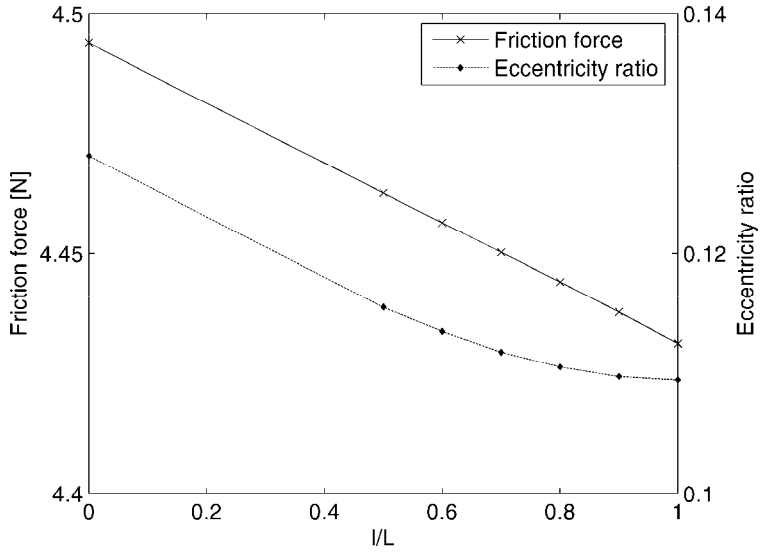


Figure 5: Friction force and eccentricity ratio for light loading

From [9], texturing the inlet of a contact can increase the load carrying capacity. The texture is the most efficient when located outside of any recirculation zone and when the texture is as deep as possible but without any backflow inside. Mechanical losses are then reduced at the inlet of the contact enabling more energy to be used for building up the pressure. Although the present case is different from a 2D slider since it is a closed system with 3D effects, this principle remains. The texture is located at the maximum film thickness where the pressure builds up. No backflow is observed for the cases considered. The texture reduces the losses at this place and thus increases the load carrying capacity of the contact. To compensate and to fulfill the force balance, the eccentricity reduces, giving a larger minimum film thickness. The new pressure profile in the mid-plan of the bearing can be seen in Figure 6. The resulting friction force is reduced not only because of the decrease in eccentricity ratio but also by the local decrease of the shear stress in the grooves. This reduction in friction force seems linear with the groove length, Figure 5. The friction force is reduced by up to 1.4% when the groove length reaches the bearing length.

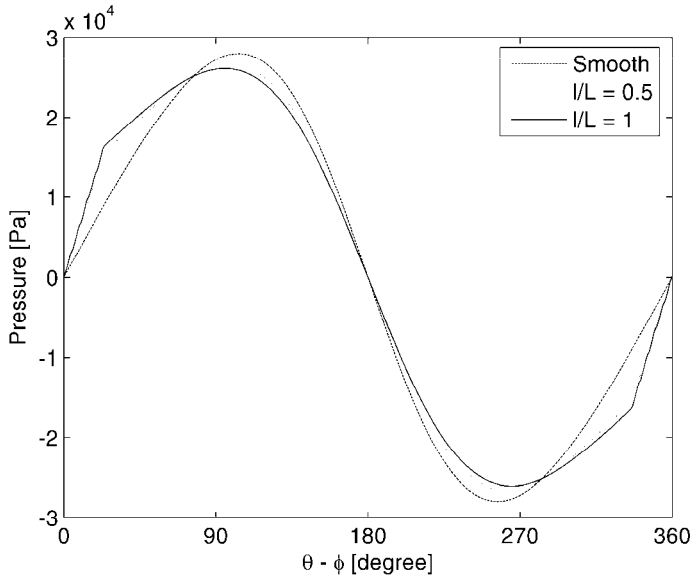


Figure 6: Pressure profile in the mid-plan, from $\theta = 90°$

It should be noted that this texture can bring even better performance if the depth is optimized at the limit of the appearance of the recirculating flow. Cavitation may appear by increasing the load, the attitude angle ($\phi$) of 90° will start to vary in this case and the position of the texture might have to be reconsidered since the texture will not be located at the maximum film. At the equilibrium position, the maximum film would be displaced on the upstream side of the texture, i.e. at lower values of $\phi$. The location may not appear as optimal. On the other hand, backflow may start to occur at the maximum film thickness. Thus, slightly shifting the texture downstream, outside of this zone (at higher $\phi$ values relative to the maximum film thickness), would be beneficial. This textured bearing can still provide improvements at higher eccentricities. For the highest eccentricities, the texture will not be efficient since too much recirculation flow will be present [8].

**High loading**

The bearing is loaded with 1125 N and released. For the textured case, the grooves are taken such that $l/L$ = 0.1, 0.2, 0.3 and 0.4. In [8], deep dimples located in the high pressure zone are able to decrease to a greater extent the friction force than the load carrying capacity thus providing a lower friction coefficient. Different results are expected when the film thickness is recalculated since a loss in load carrying capacity would produce a decrease in minimum

film and consequently an increase in friction force. The question is whether the friction force is still going to be lower with the recalculated film or not?

From Figure 7, it can be seen that friction force decreases when the groove length increases. This reduction goes together with an increase of the eccentricity ratio, i.e. a reduction of the minimum film. As the grooves reduce the load carrying capacity, see [8], the equilibrium position has to be at a higher eccentricity in order to compensate this effect. Compared with the smooth bearing, the local thicker film in the grooves reduces friction to a greater extent. Grooves contribute to lower losses even though the bearing operates at higher eccentricity.

The maximum pressure decreases with the groove length as the pressure is cut off by the grooves, Figure 8. The maximum pressure zone is then spread over the groove area, Figure 9. It should also be noted that the attitude angle is varied by less than 1.5° between these different cases. The drawback of having long grooves in the axial direction for a static case (when the film is fixed) no longer remains: contrary to the static case where long grooves provide more side leakage and a great loss in pressure, the maximum pressure zone does not significantly decrease when the lubricant film is recalculated as the bearing has to sustain the same load. Compensation is made by reducing the minimum film thickness.

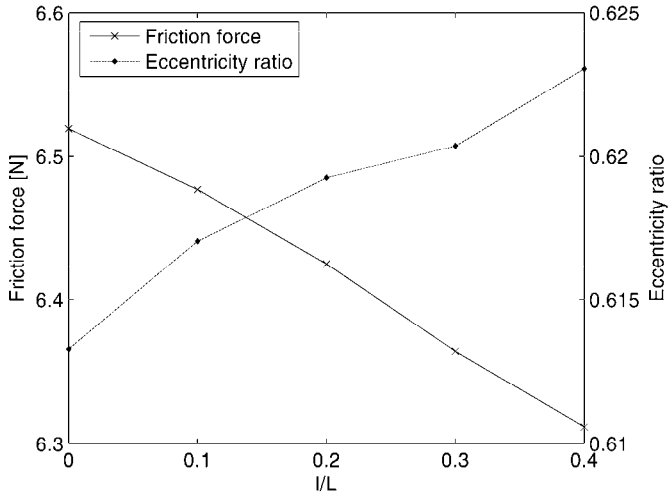


Figure 7: Friction force and minimum film for high loading

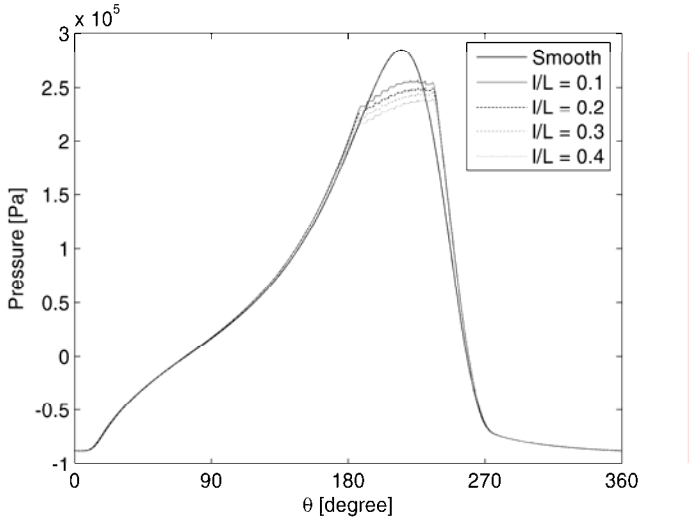


Figure 8: Pressure profile in the mid-plan

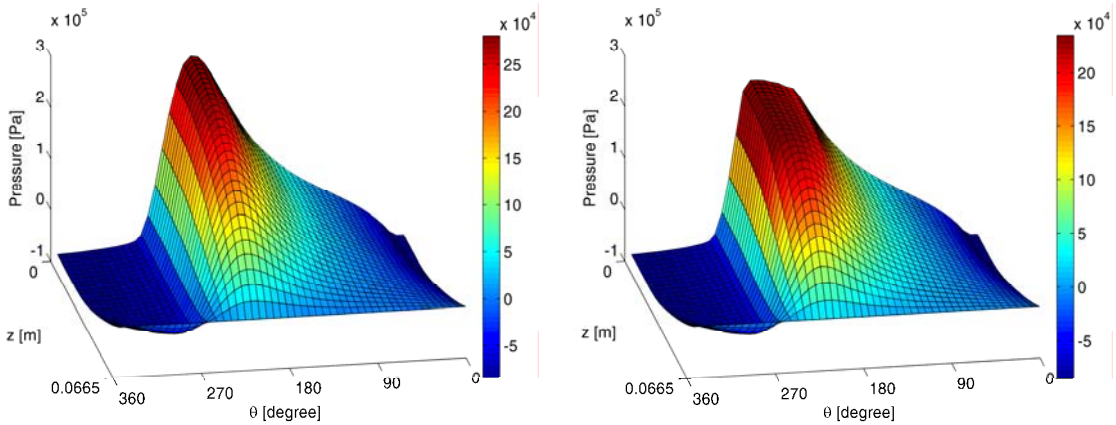


(a) Smooth bearing (b) Textured bearing ($l/L$ = 0.4)

Figure 9: 3D pressure profile

Before claiming that this texturing is beneficial for reducing friction, another aspect needs to be examined. Reducing the minimum film thickness in order to get a lower friction force is a goal that a thinner lubricant can achieve. A lubricant with lower viscosity carries less load, contributing thus to a thinner film and lower friction force at the equilibrium position (steady state). This solution has to be compared with the texturing performance as it would be much easier to replace a lubricant than to texture the bearing. To check this, a smooth bearing is tested with a lubricant having a lower dynamic viscosity. The eccentricity is fixed and equal to the eccentricity of the textured bearing with $l/L_z$ = 0.4. The viscosity is varied in order to find the value that gives the applied load of 1125 N. For this particular viscosity, the resulting friction force is compared with the friction force of the textured bearing. This gives then a fair comparison between these two alternatives. From Figure 10, the dynamic viscosity needs to be reduced by about 3% to give the same applied load. The friction force is about 6.42 N which represents a 1.7% higher friction compared with the textured bearing.

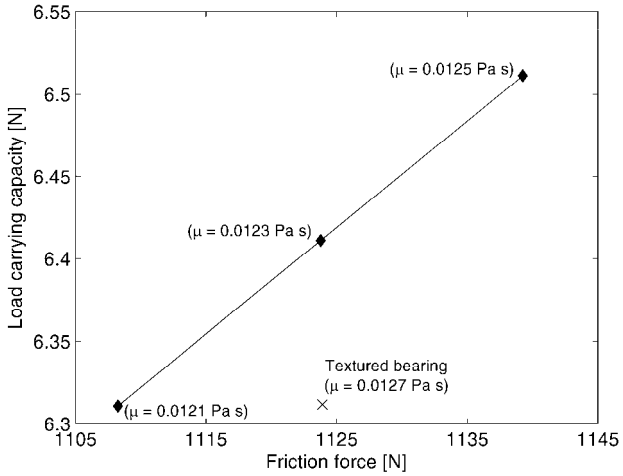


Figure 10: Friction force for a smooth bearing with thinner lubricant

If these two cases were compared at the same friction force, the viscosity used for the smooth bearing would have been even lower, the load carrying capacity would have been reduced and the fluid film would have ended up at a lower value than that of the textured bearing with initial viscosity. It can thus be concluded that, in the case considered, texturing of the bearing surface is a more efficient way to decrease friction compared to the use of a thinner lubricant.

## CONCLUSION

The recalculation of the fluid film by a motion of the grid nodes is essential to analyse the performance of such textured bearings. From this study, the following conclusions can be drawn:

• For light loading conditions, texturing the bearing with shallow grooves in the maximum film zone confirms the trend observed in [8]. The minimum film thickness is increased and friction force is reduced.

• For high loading conditions, texturing the bearing surface with deep grooves in the maximum pressure zone reduces the friction force. The lubricant minimum film becomes nevertheless lower.

• The texture located in the maximum pressure zone provides better reduction in friction force than a smooth bearing operating with a thinner lubricant.


## ACKNOWLEDGEMENT

The authors would like to acknowledge the financial support provided by the Swedish Research Council (Vetenskapsrådet).


## REFERENCES


[1] ETSION, I., 2005. "*State of the art in laser surface texturing*". Journal of Tribology, 127(1), pp. 248–253.

[2] LIN, T.-R., 1994. "*Steady state performance of finite hydrodynamic journal bearing with three-dimensional irregularities*". Wear, 176(1), pp. 95–102.

[3] LI, H., and BRAUN, M.J., 2007. "*The lubricant flow structure and pressure generation in a journal bearing with diamond-knurled stator surface*". In Proceedings of the ASME Turbo Expo 2007 - Power for Land, Sea, and Air, Vol. 5, pp. 1005–1015.

[4] KATO, T., and OBARA, S., 1996. "*Improvement in dynamic characteristics of circular journal bearings by means of longitudinal microgrooves*". Tribology Transactions, 39(2), pp. 462– 468.

[5] KUMADA, Y., HASHIZUME, K., and KIMURA, Y., 1996. "*Performance of plain bearings with circumferential microgrooves*". Tribology Transactions, 39(1), pp. 81–86.

[6] AUSAS, R., RAGOT, P., LEIVA, J., JAI, M., BAYADA, G., and BUSCAGLIA, G.C., 2007. "*The impact of the cavitation model in the analysis of microtextured lubricated journal bearings*". Journal of Tribology, 129(4), pp. 868–875.

[7] TALA-IGHIL, N., MASPEYROT, P., FILLON, M., and BOUNIF, A., 2007. "*Effects of surface texture on journal-bearing characteristics under steady-state operating conditions*". Proceedings of the Institution of Mechanical Engineers, Part J: Journal of Engineering Tribology, 221(6), pp. 623–633.

[8] CUPILLARD, S., GLAVATSKIH, S., and CERVANTES, M.J., 2008. "*Computational fluid dynamics analysis of a journal bearing with surface texturing*". Proc. IMechE, PartJ: J. Engineering Tribology, 222(J2), pp. 97–107.

[9] CUPILLARD, S., CERVANTES, M.J., and GLAVATSKIH, S., 2008. "*Pressure build-up mechanism in a textured inlet of a hydrodynamic contact*". Journal of Tribology, 130. 021701.

[10] JAKOBSSON, B., and FLOBERG, L., 1957. *The finite journal bearing, considering vaporization*, Vol. 190. Chalmers Tekniska Högskolas Handlingar.

[11] ALMQVIST, T., and LARSSON, R., 2002. "*The Navier-Stokes approach for thermal EHL line contact solutions*". Tribology International, 35(3), pp. 163–170.

[12] BERGSTRÖM, J., and GEBART, R., 1999. "*Estimation of numerical accuracy for the flow field in a draft tube*". International Journal of Numerical Methods for Heat and Fluid Flow, 9(4), pp. 472–486.